Fabrication and Characterization of a Miniaturized 15-MHz Side-Looking Phased-Array Transducer Catheter

Nestor E. Cabrera-Munoz, *Member, IEEE*, Payam Eliahoo, Robert Wodnicki, *Member, IEEE*, Hayong Jung, Chi Tat Chiu, Jay A. Williams, Hyung Ham Kim, *Member, IEEE*, Qifa Zhou, *Fellow, IEEE*, Guang-Zhong Yang, *Fellow, IEEE*, and K. Kirk Shung, *Life Fellow, IEEE*

***Abstract*— This paper describes the development of a miniaturized 15-MHz side-looking phased-array transducer catheter. The array features a 2–2 linear composite with 64 piezoelectric elements mechanically diced into a piece of PMN-30% PT single crystal and separated by nonconductive epoxy kerfs at a 50-μm pitch, yielding a total active aperture of 3.2 mm in the azimuth direction and 1.8 mm in the elevation direction, with an elevation natural focal depth of 8.1 mm. The array includes nonconductive epoxy backing and two front matching layers. A custom flexible circuit connects the array piezoelectric elements to a bundle of 64 individual 48-AWG microcoaxial cables enclosed within a 1.5-m-long 10F catheter. Performance characterization was evaluated via finite-element analysis simulations and afterward compared against obtained measurement results, which showed an average center frequency of 17.7 MHz, an average bandwidth of 52.2% at −6 dB, and crosstalk less than −30 dB. The imaging of a tungsten fine-wire phantom resulted in axial and lateral spatial resolutions of approximately 90 and 420 μm, respectively. The imaging capability was further evaluated with colorectal tissue-mimicking phantoms, demonstrating the potential suitability of the proposed phased-array transducer for the intraoperative assessment of surgical margins during minimally invasive colorectal surgery procedures.**

***Index Terms*— High-frequency imaging, materials/technology for medical transducers, piezoelectric and ferroelectric transducer materials, transducer modeling [finite-element analysis (FEA) and analytical].**

Manuscript received June 16, 2018; accepted March 15, 2019. Date of publication March 20, 2019; date of current version June 5, 2019. This work was supported in part by NIH under Grant P41-EB002182 and in part by U.K. Engineering and Physical Sciences Research Council (EPSRC). *(Corresponding author: Nestor E. Cabrera-Munoz.)*

N. E. Cabrera-Munoz, P. Eliahoo, R. Wodnicki, H. Jung, Q. Zhou, and K. K. Shung are with the Department of Biomedical Engineering, University of Southern California, Los Angeles, CA 90089 USA (e-mail: cabreram@usc.edu).

C. T. Chiu was with the Department of Biomedical Engineering, University of Southern California, Los Angeles, CA 90089 USA. He is now with the Department of Imaging and Bioelectronics, General Electric Global Research, Niskayuna, NY 12309 USA.

J. A. Williams, retired, was with the Department of Biomedical Engineering, University of Southern California, Los Angeles, CA 90089 USA. He resides in Lemont, PA 16851 USA.

H. H. Kim was with the Department of Biomedical Engineering, University of Southern California, Los Angeles, CA 90089 USA. He is now with the Department of Creative IT Engineering, Pohang University of Science and Technology, Pohang 37673, South Korea.

G.-Z. Yang is with the Hamlyn Centre for Robotic Surgery, Imperial College London, London SW7 2AZ, U.K.

Digital Object Identifier 10.1109/TUFFC.2019.2906134

I. Introduction

MINIMAL access surgery (MAS) has become a popular surgical discipline through which patients undergo reduced trauma and recovery time without compromising the safety and efficacy obtained with traditional open surgery approaches [1]. Because of the minimally invasive access, visualization of the area under treatment becomes a challenge.

Imaging modalities such as magnetic resonance imaging (MRI) and computed tomography (CT) produce good quality images with good contrast resolution and a relatively large field of view; however, a major drawback is that they are not performed intraoperatively since the imaging equipment is bulky and incompatible with the operating theater [2]. As a result, miniaturized interventional devices with imaging capabilities have been developed to fulfill the intraoperative visualization needs of areas undergoing MAS procedures.

Ultrasound imaging is safe and portable with the advantage that the probe itself can be interventional. Interventional ultrasound probes include miniaturized ultrasonic transducers attached to their distal ends. The intended MAS procedures ultimately determine their design requirements, such as number of elements, aperture size, frequency, and viewing orientation, with their construction presenting a number of technical challenges particularly related to electrical interconnects and packaging [3].

For example, Cummins *et al.* [4] recently developed a miniaturized 60 MHz, side looking (SL), 64-element linear array considering required penetration depth and dimensional constraints for a breast biopsy needle.

There are also miniaturized probes that combine ultrasound with multiple imaging modalities into a single interventional device. One example developed by Yang *et al.* [5] integrates ultrasound with optical coherence tomography (OCT) and photoacoustic tomography to provide tissue information at different depths and resolutions for ovarian tissue characterization.

Furthermore, miniaturized imaging probes have successfully been combined with minimally invasive robotic surgery instruments [6]. One example being developed by the Hamlyn Centre for Robotic Surgery, Imperial College London, London, U.K., features an endomicroscopy probe mounted on a novel robotic surgical arm which provides colorectal surgeons with

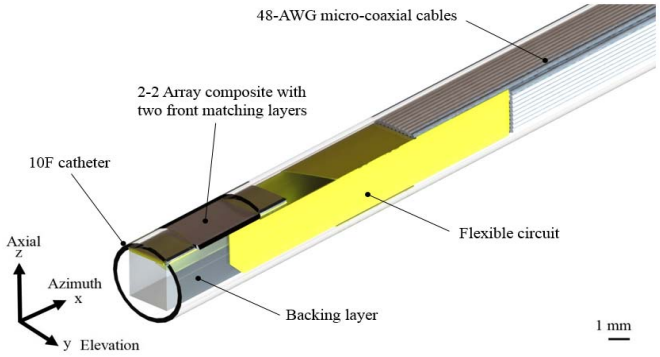

Fig. 1. CAD model of the SL-ERUS phased-array transducer enclosed in the protective 10F catheter.

TABLE I
SL-ERUS PHASED-ARRAY TRANSDUCER DESIGN PARAMETERS

Design center frequency	15 MHz
Number of elements	64
Composite configuration	2-2, linear
Pitch	50 μm (0.5 λwater)
Element width	37 μm
Kerf width	13 μm
Elevation aperture	1.8 mm
Azimuth aperture	3.2 mm
Elevation natural focal distance	8.1 mm
Piezoelectric material	PMN-30%PT (53 μm thick)
Kerf filler material	Epo-Tek 301 (53 μm thick)
Backing layer material	Epo-Tek 301 + 43.2 wt% LP-3 (2 mm thick)
1st Matching layer material	2,3-μm silver epoxy (45 μm thick)
2nd Matching layer material	Parylene C (30 μm thick)

cellular level information at the surface of the colorectal wall undergoing transanal endoscopic microsurgery (TEM) [7].

Such robotic surgical arm also enables the integration of a miniaturized endorectal ultrasound (ERUS) probe with a packaging diameter smaller than 3.5 mm to additionally provide depth-resolved information below the colorectal wall. However, current commercially available ERUS probes have diameters larger than 15 mm [8].

This paper discusses the fabrication and characterization of a miniaturized 15 MHz, SL, 64-element phased-array transducer packaged within a 10F catheter that can be integrated with the aforementioned robotic surgical instrument. This miniaturized array transducer offers adequate penetration depth and spatial resolutions for its potential application to detect solid structures and cysts present in colorectal tissue.

II. ARRAY TRANSDUCER DESIGN

The SL-ERUS phased-array transducer catheter construction was 3-D modeled via the computer-aided design (CAD) software SolidWorks (Dassault Systèmes SolidWorks Corporation, Vélizy-Villacoublay, France) considering dimensional requirements of the robotic surgical instrument. As shown in Fig. 1, such instrument required the array to be enclosed within a 10F catheter having an external diameter of 3.3 mm. The array acoustic stack is connected to a custom flexible circuit that clamps the 2–2 composite on its proximal and distal ends to provide ground connection. The design of the flexible circuit allows connecting and fitting a bundle of 64 individual 48-American Wire Gauge (AWG) microcoaxial cables inside of the catheter to excite each one of the piezoelectric elements. The array does not include a lens to enable colorectal surgeons to image the full thickness of the colorectal wall ($>$ 6 mm) [9], while delicately manipulating the instrument within the colorectal cavity.

A. Array Acoustic Stack

The center frequency of the array was chosen to be 15 MHz to achieve adequate penetration depth and spatial resolutions necessary to reliably visualize the full thickness of the colorectal wall. Lead magnesium niobate-30% lead titanate (PMN-30% PT) (CTS Corporation, Bolingbrook, IL, USA) single crystal was chosen as the piezoelectric material due to its high dielectric constant and low dielectric loss, which makes it ideal for high sensitivity transducers with small aperture size [10].

The array 2–2 composite consists of sixty-four 37-μm-wide piezoelectric elements separated by 13-μm-wide kerfs filled with nonconductive epoxy, Epo-Tek 301 (Epoxy Technology, Inc., Billerica, MA, USA), to yield an array with a 50-μm-wide pitch ($0.5\lambda_{\text{water}}$ pitch for the suppression of undesirable grating lobes during beam steering [11]), a total active azimuth aperture of 3.2 mm, and a total active elevation aperture of 1.8 mm with a natural focal distance of 8.1 mm.

The array acoustic stack includes a backing layer of nonconductive epoxy, Epo-Tek 301, mixed with 43.2 wt% liquid plasticizer, LP-3 (Structure Probe, Inc., West Chester, PA, USA), and two front matching layers: 1) silver-loaded epoxy consisting of 2, 3-μm silver powder (Aldrich Chemicals Co., St. Louis, MO, USA) with mixed epoxy, Insulcast 501 + Insulcure 9 (ITW Polymers Coatings North America, Montgomeryville, PA, USA) and 2) vapor-deposited polymer, Parylene C (Specialty Coating Systems, Inc., Indianapolis, IN, USA). The array design parameters and material properties are shown in Tables I and II, respectively.

B. Flexible Printed Circuit

The number of elements, their width and pitch, and the available space inside of the 10F catheter required designing a high-density flexible printed circuit. Fig. 2(a) shows the CAD schematics (AutoCAD, Autodesk, Inc., San Rafael, CA, USA) of the flexible circuit design that allows connecting and fitting a bundle of 64 individual 48-AWG microcoaxial cables inside of the 10F catheter to excite each one of the 64 piezoelectric elements.

The flexible circuit features sixty-four 30-μm-wide signal traces with a 50-μm-wide pitch on the 2–2 array composite area, divided into two groups of 32 signal traces each. Each group further divides into three branches of 10 (center tab) or 11 (side tabs) signal traces, each of which will then be connected to an individual 48-AWG microcoaxial cable. Connection pads are 100-μm wide and their pitch is 180 μm. Fig. 2(b) shows the folding sequence of the flexible circuit:

TABLE II
MATERIAL PROPERTIES OF THE SL-ERUS PHASED-ARRAY TRANSDUCER ACOUSTIC STACK

Material	PMN-30%PT single crystal[1]	Epo-Tek 301[2]	Epo-Tek 301 + 43.2 wt% LP-3[3]	2,3-µm silver epoxy[3]	Parylene C[4]
Density, ρ (kg/m^3)	7,800	1,150	1,230	3,860	1,100
Acoustic longitudinal velocity, c (m/s)	4,600	2,650	2,450	1,900	2,350
Acoustic impedance, Z (MRayl)	35.88	3.05	3.01	7.33	2.59
Piezoelectric strain constant, d_{33} (C/N)	1,500 x 10^{-12}	-	-	-	-
Free dielectric constant, K^{ε}	~5,000	-	-	-	-
Clamped dielectric constant, K^{ε}	800	-	-	-	-
Dielectric loss tangent, tanδ_e	0.005	-	-	-	-
Electromechanical coupling coefficient, k_t	0.58	-	-	-	-

1. CTS Corporation, Bolingbrook, IL, USA.
2. Epoxy Technology, Inc., Billerica, MA, USA.
3. Resource Center for Medical Ultrasonic Transducer Technology at the University of Southern California, Los Angeles, CA, USA.
4. Specialty Coating Systems, Inc., Indianapolis, IN, USA.

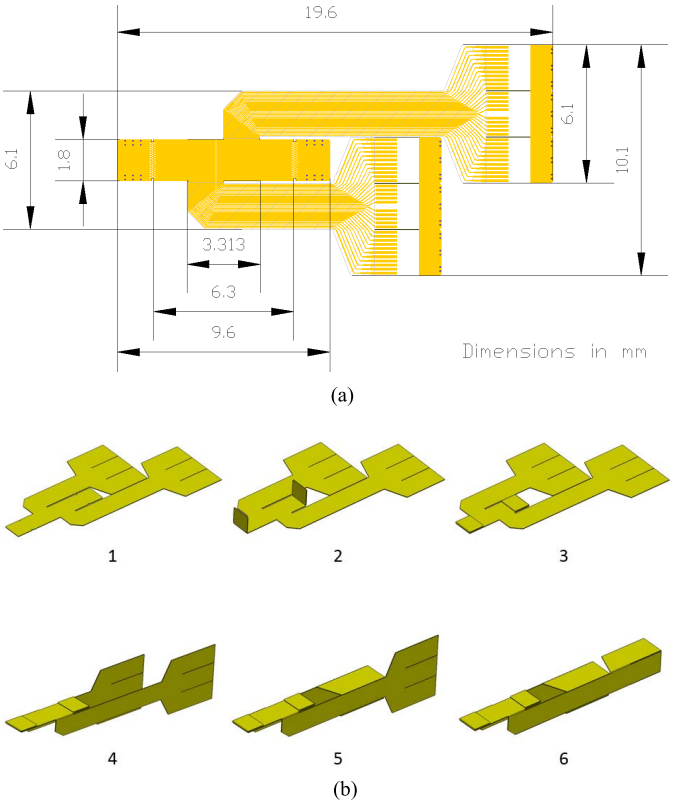

Fig. 2. (a) CAD schematics of flexible printed circuit design. (b) Folding sequence of the flexible printed circuit.

1—flat state, 2–3—fold composite clamping flaps, 4—fold two main branches, 5—fold side tabs of the first main branch, and 6—fold side tabs of the second main branch.

C. Microcoaxial Cable

The microcoaxial bundle features 64 individual 48-AWG microcoaxial cables (#5481-120, Hitachi Metals, Ltd., Tokyo, Japan). The microcoaxial cable was first characterized to determine its impedance, Z_o, and propagation constant, γ, at 15 MHz based upon the following formula for a microcoaxial cable of length x [12]:

$$Z_x = Z_o \frac{[Z_{\text{load}} + Z_o \tanh(\gamma x)]}{[Z_o + Z_{\text{load}} \tanh(\gamma x)]} \tag{1}$$

where Z_{load} represents the electrical impedance of the transducer and Z_x is the transformed coaxial impedance measured on the system end of the cable. The values for Z_o and γ were obtained by measuring the complex open- and short-circuit impedance for a sample cable on an Agilent E4991A RF Impedance/Material Analyzer (Agilent Technologies, Santa Clara, CA, USA). As done by Cannata *et al.* [13], the complex transformed impedance was recorded for both the short-circuit and the open-circuit Z_{load} values [13]. The two measured values for Z_x and (1) were then used to solve for Z_o and γ. The distributed network representation for the microcoaxial cable was also solved [14]. The resultant per-unit-length values of cable propagation velocity (v), DC resistance (r), series inductance (l), shunt capacitance (c), and attenuation (α) were recorded and are listed in Table III.

TABLE III
MEASURED PROPERTIES OF THE 48-AWG MICROCOAXIAL CABLE AT 15 MHz

Property	Hitachi #5481-120		
Characteristic impedance, Z_o	52.59 - 22.63i Ω		
Propagation constant, γ	0.24 + 0.57i m^{-1}		
Propagation velocity, v	1.6 x 10^8 m/s		
DC resistance / unit length, r	21.3 Ω/m		
Series inductance / unit length, l	0.12 µH/m		
Shunt capacitance / unit length, c	127 pF/m		
Attenuation / unit length, α	2.08 dB/m		
	1.5 m	2.0 m	2.4 m
Reflection coefficient, S_{11} (dB)	-11.56	-11.01	-10.99
Transmission coefficient, S_{21} (dB)	-3.18	-4.21	-5.08

In order to determine the optimal microcoaxial cable length to be used, scattering parameters (S-parameters) were evaluated to achieve the best performance in terms of reflection and transmission [15].

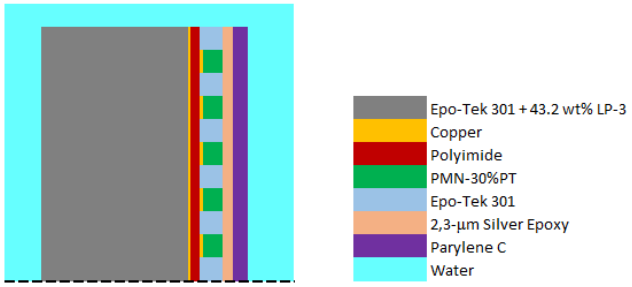

Fig. 3. Section of the FEA model illustrating the simulated layers.

The S-parameters of the 48-AWG microcoaxial cable were measured at three different cable lengths considering minimum and maximum cable length requirements provided by the Hamlyn Centre for Robotic Surgery. These measurements were performed under no-load conditions with the microcoaxial cable connected to the two 50-Ω ports of an Agilent E5072A Network Analyzer (Agilent Technologies, Santa Clara, CA, USA). Table III shows the effect of the microcoaxial cable length on the S-parameters. At 15 MHz, the reflection coefficient, S_{11}, increases with increasing cable length. A 1.5-m cable length generates less reflection at the input and output; therefore, having less oscillatory effect on the transmitted and received signal. At 15 MHz, the transmission coefficient, S_{21}, decreases with increasing cable length. In other words, the loss of the transmitted signal increases with increasing cable length. Therefore, the measurements denote what is expected from a lossy transmission line model and clearly indicate that 1.5-m cable length delivers higher power to drive the array transducer.

D. Array Transducer Simulation Modeling

The SL-ERUS phased-array transducer was simulated via a 2-D finite-element analysis (FEA) model (PZFlex, Weidlinger Associates, Inc., Cupertino, CA, USA) to predict its performance, and therefore reduce the number of time-consuming prototype fabrication runs [16]. The array performance was evaluated and optimized via standard nonimaging simulations that included electrical impedance, pulse-echo response, as well as combined electrical and acoustical crosstalk. Fig. 3 shows a section of the FEA model illustrating the simulated layers. The Field II program was used to simulate the one-way azimuthal directivity response of a single array element [17] and to estimate the effective element width. Krimholtz–Leedom–Matthaei (KLM) modeling (PiezoCAD, Sonic Concepts, Inc., Bothell, WA, USA) was used to simulate the insertion loss of a single array element. Comparisons of simulated results against measured results are presented below in Section VI.

III. Array Transducer Fabrication

A. Array Acoustic Stack

The array 2–2 composite was fabricated using the dice-and-fill technique described by Savakus *et al.* [18]. At CTS Corporation (CTS Corporation, Bolingbrook, IL, USA), kerfs were mechanically cut with a dicing saw (0.5-mm/s feed rate and 40 000 r/min spindle speed) into a plate of bulk PMN-30% PT and backfilled with Epo-Tek 301 epoxy. The diced-and-filled PMN-30% PT plate was then shipped to our group, the Resource Center for Medical Ultrasonic Transducer Technology, University of Southern California, Los Angeles, CA, USA. One of its sides was then lapped down using 2000-grit sandpaper together with 9-μm aluminum oxide (Al_2O_3) powder (Buehler-Illinois Tool Works, Inc., Lake Bluff, IL, USA) to ensure a smooth and matte finish. Lapping with 9-μm diamond suspension, MetaDi (Buehler-Illinois Tool Works, Inc., Lake Bluff, IL, USA), was done at the end to remove any excess of kerf filler epoxy, and make sure that the whole first lapped side of the piece was completely flat.

Afterward, the sample was mechanically cleaned by applying acetone, reagent alcohol, and Alconox detergent (Alconox, Inc., White Plains, NY, USA) with a cotton swab and any residues left were removed with deionized water. The lapped and mechanically cleaned side of the 2–2 composite was then plasma cleaned (argon 25 sccm, 30 W, and 185 s) to activate the exposed surface of the piezoelectric elements for electroplating sputtering of their active electrodes having a thickness of 500 Å of chrome and 2000 Å of gold. Since electroplating sputtering actually covered the whole top surface of the 2–2 composite, the active electrodes were patterned on the piezoelectric elements by removing gold and chrome from the epoxy kerfs with a cotton swab dampened in reagent alcohol, taking advantage of the weak adhesion of chrome and gold to epoxies.

The 2–2 composite was then flipped over and lapped down to its final design thickness. Again, 2000-grit sandpaper together with 9-μm Al_2O_3 powder were used to ensure a smooth and matte finish, and 9-μm diamond suspension lapping was done to remove any excess of kerf filler epoxy. After undergoing the same process of mechanical and plasma cleaning, the 2–2 composite had its common ground sputtered having a thickness of 500 Å of chrome and 2000 Å of gold.

The first matching layer was then prepared by adding 4.5 g of 2, 3-μm silver powder to 1.25 g of mixed nonconductive epoxies Insulcast 501 and Insulcure 9. The resulting mixture was then degassed to avoid the presence of air bubbles, cast on top of the common ground electrode, and centrifuged at 3000 r/min for 15 min to distribute it evenly. After curing overnight in a dry-environment nitrogen box and postcuring in a forced convection oven for 2 h at 45 °C, the first matching layer was lapped down to its final design thickness and the resulting acoustic stack (2–2 composite + first matching layer) was mechanically diced (0.5-mm/s feed rate and 30 000-r/min spindle speed) to final dimensions, as shown in Fig. 4.

B. Flexible Printed Circuit

The two-layer flexible printed circuit was fabricated by MicroConnex (MicroConnex Corp., Snoqualmie, WA, USA). Fig. 5 shows a physical sample of the flexible circuit consisting of a 25-μm-thick base dielectric polyimide layer, Kapton (DuPont, Wilmington, DE, USA), which features signal traces on the front (cover-layer protected along the main branches) and an exposed common ground electrode on the back with

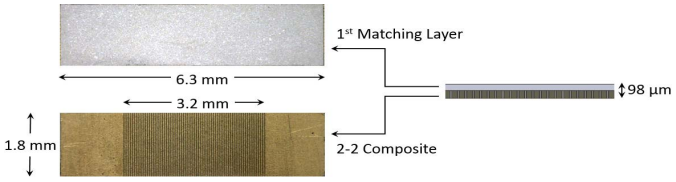

Fig. 4. Acoustic stack comprising the PMN-30% PT 2–2 composite and the first matching layer. Active and ground electrodes were sputtered on the bottom and top sides of the composite, respectively. Both layers were lapped down to final design thicknesses and the resulting stack was mechanically diced to final dimensions.

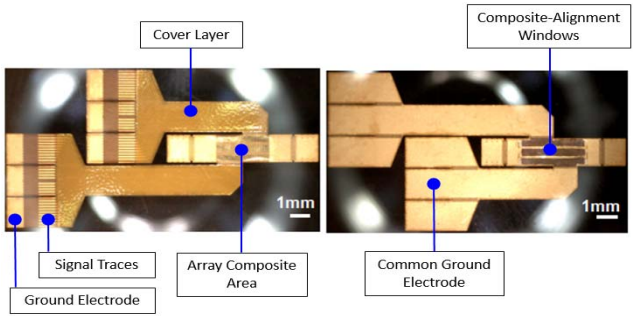

Fig. 5. Flexible printed circuit for the SL-ERUS phased-array transducer. (a) Frontside with cover-layer protected signal traces. (b) Backside with exposed common ground electrode featuring three windows for 2–2 composite proper alignment and positioning.

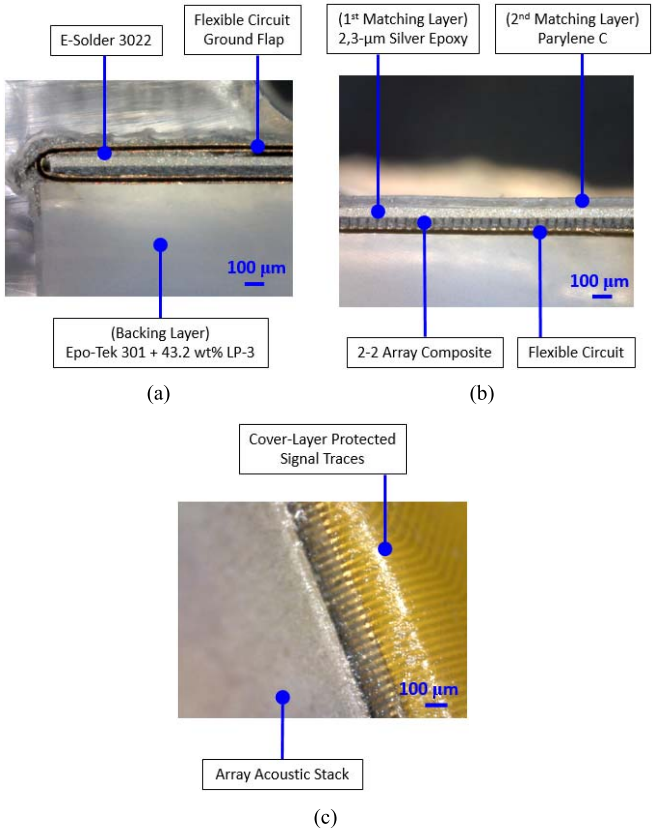

Fig. 6. (a) and (b) Cross-sectional images revealing the diverse components of the array acoustic stack and backing layer bonded to the flexible circuit. (c) Detail view of the bending of one main branch of the flexible circuit, making sure there were no broken signal traces.

etched transparent windows that reveal the polyimide layer for 2–2 composite proper alignment and positioning. All signal traces and ground electrodes were patterned over a 4-μm-thick copper layer and finished with a flash of gold.

C. Assembling the Array Acoustic Stack-Flexible Printed Circuit-Backing Layer Module

After mechanical dicing to final dimensions, both sides of the resulting array acoustic stack were cleaned by applying trichloroethylene, acetone, and reagent alcohol with a cotton swab. Similarly, the frontside of the flexible circuit was cleaned with a cotton swab dampened in reagent alcohol. Afterward, a thin line of Epo-Tek 301 epoxy was applied with a foam swab at the center of the flexible circuit, on the 2–2 composite area. Another foam swab was used then to smear a thin layer of Epo-Tek 301 epoxy all over the surface of the 2–2 composite (bottom side of the array acoustic stack).

The acoustic stack was afterward placed on the top of the flexible circuit visually making sure that the piezoelectric elements were correctly aligned with the signal traces, and pressure was applied using a "C" clamp. The resulting subassembly was cured overnight in a dry-environment nitrogen box and then postcured in a forced convection oven for 2 h at 45 °C.

The next step involved bonding the backing layer to the backside of the flexible circuit. For this purpose, the backside of the flexible circuit was cleaned with a cotton swab dampened in reagent alcohol. Afterward, a thin line of Epo-Tek 301 epoxy was applied with a foam swab at the center of the flexible circuit (backside of the 2–2 composite area) and another foam swab was used then to smear a thin layer of Epo-Tek 301 epoxy all over the bonding surface of the backing layer. The backing layer was afterward placed on the top of the flexible circuit backside, and pressure was once again applied with a "C" clamp. Similarly, the resulting subassembly was cured overnight in a dry-environment nitrogen box and then postcured in a forced convection oven for 2 h at 45 °C.

In order to connect the common ground electrode on the backside of the flexible circuit to the front matching layer, the two clamping flaps featuring metalized thru-vias were bent and then bonded to the front matching layer using conductive epoxy, E-Solder 3022 (Von Roll Isola USA, Inc., Schenectady, NY, USA). Afterward, the two main branches of the flexible circuit were bent and bonded to the sides of the backing layer using Epo-Tek 301 epoxy.

The resulting module was then all covered, excluding the soldering pads, with a 30-μm-thick layer of vapor deposited polymer, Parylene C, serving as both the second matching layer and insulation. Fig. 6 shows cross-sectional images revealing the diverse components of the assembled module and a detail view of the bending of one main branch of the flexible circuit, making sure there were no broken signal traces.

D. Microcoaxial Cable-Assembly Connection to the Flexible Printed Circuit

The 48-AWG microcoaxial cable was cut into sixty-four 1.5-m long pieces with their ends codified with colors and

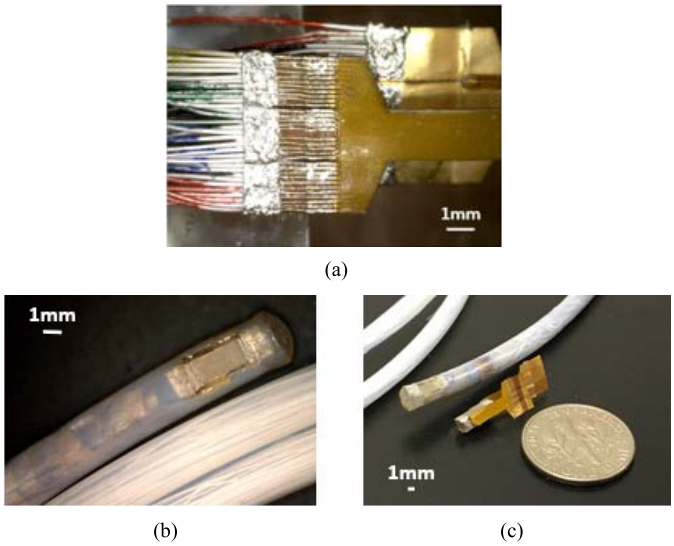

(a) (b) (c)

Fig. 7. (a) Connection of the 48-AWG microcoaxial cable assembly to the flexible printed circuit. (b) Finished distal end with a 7-μm-thick layer of vapor-deposited Parylene C to ensure complete insulation. (c) Size comparison of the finished distal end, the array acoustic stack-flexible circuit-backing layer module, and a dime coin.

a corresponding number, respectively. Afterward, all the 64 pieces were carefully pulled through a 1.45-m-long 10F polytetrafluoroethylene (PTFE) catheter and had their color ends manually stripped.

The exposed inner conductor of each single piece of 48-AWG microcoaxial cable was then carefully bonded to its respective 100-μm-wide connection pad using E-Solder 3022 epoxy. After completing the first side with the first 32 connections, Epo-Tek 301 epoxy was manually applied over the three flexible circuit tabs to pot and protect the connections created. More E-Solder 3022 epoxy was then manually applied to bond the exposed outer conductors to the ground pads of each of the three flexible circuit tabs. The same process was repeated for the second side with the remaining 32 connections. Fig. 7(a) shows a photograph of all 64 connections completed.

For larger scale manufacturing, resistance welding with parallel-gap fine tip could be implemented to expedite soldering of the microcoaxial cable assembly to the flexible circuit. Furthermore, flexible transmission lines on liquid-crystal polymer (LCP) offering comparable signal integrity to microcoaxial cable could also be developed and be brought down the length of the catheter [19].

E. Final Packaging and Connection to Imaging System Connector

After completing all connections, the flexible circuit was folded into its final configuration and carefully pulled inside the distal end of the 10F PTFE catheter. The array aperture was then positioned right in the center of a manually precut window (3.7 mm $\times$ 2.2 mm) on the distal end of the catheter. Epo-Tek 301 epoxy was applied to fill in the gaps between the array acoustic stack-flexible circuit-backing layer module and the edges of the window, as well as to seal the opening at the tip of the catheter.

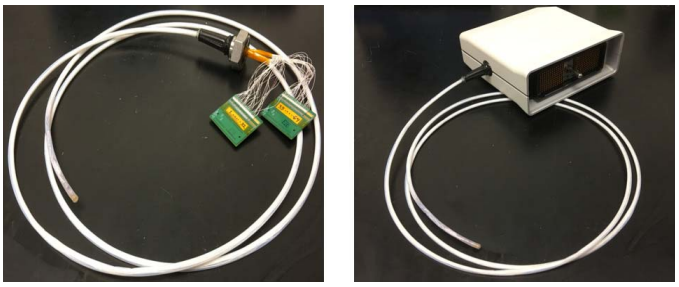

(a) (b)

Fig. 8. (a) SL-ERUS phased-array transducer finished with a pair of Verasonics microcoaxial termination boards, each one handling 32 channels. (b) SL-ERUS phased-array transducer connected to Verasonics Backshell Connector.

Afterward, a 7-μm-thick layer of Parylene C was vapor deposited to ensure complete insulation of the distal end of the SL-ERUS phased-array transducer catheter, as shown in Fig. 7(b). A size comparison of the distal end of the SL-ERUS phased-array transducer catheter, the array acoustic stack-flexible circuit-backing layer module, and a dime coin is shown in Fig. 7(c).

The proximal end of the cable assembly was then connected with E-Solder 3022 epoxy to a pair of Verasonics microcoaxial termination boards (Verasonics, Inc., Kirkland, WA, USA), each one handling 32 microcoaxial cables. All the connections were potted with Epo-Tek 301 epoxy for protection, leaving exposed just the top surface of the resulting E-Solder 3022 epoxy electrodes for posterior poling and testing. Fig. 8(a) shows the two bundles of 32 microcoaxial cables, each held together with a piece of polyimide tape, bonded with Epo-Tek 301 epoxy to a black polyvinyl chloride (PVC) cable strain relief boot (Amphenol Corporation, Wallingford, CT, USA), and finished with a Verasonics M14-A2-70 Hex cable strain relief nut.

The pair of Verasonics microcoaxial termination boards was then connected to a Verasonics Backshell Connector, following Verasonics channel mapping to avoid any drawback when connecting the array transducer to a Verasonics Vantage imaging system. Fig. 8(b) shows the completely finished SL-ERUS phased-array transducer catheter.

IV. Array Transducer Characterization

A. Electrical Impedance

Before connecting the array acoustic stack-flexible circuit-backing layer module to the microcoaxial cable assembly, each one of the 64 piezoelectric PMN-30% PT elements was individually repolarized in air at room temperature under an electric field of 20 kV/cm for 3 min using a Spellman–Bertan Model 210-02R high voltage power supply (Spellman High Voltage Electronics Corporation, Hauppauge, NY, USA). The electrical impedance of each individual array element was then measured using its respective flexible circuit signal and ground electrodes as probing pads with an Agilent E4991A RF Impedance/Material Analyzer (Agilent Technologies, Santa Clara, CA, USA) and both the magnitude and phase angle

were recorded over the frequency range of the array transducer passband.

B. Pulse-Echo Response and Insertion Loss

Upon fabrication completion of the SL-ERUS phased-array transducer catheter, the 64 piezoelectric PMN-30% PT elements were once again individually repolarized under the same aforementioned conditions. Afterward, the pulse-echo response of each individual array element was recorded to determine its effective center frequency, −6-dB fractional bandwidth (BW), peak-to-peak sensitivity, and pulse length (PL).

This test was performed by immersing the SL-ERUS phased-array transducer catheter in a deionized water tank containing a polished quartz reflector as the target at the elevation natural focal distance of 8.1 mm. The pulser/receiver used was a Panametrics-NDT 5900PR (Panametrics, Inc., Waltham, MA, USA), which emitted single-cycle unipolar pulses with an amplitude of −100 V at a pulse repetition frequency (PRF) of 200 Hz. Energy and damping were set at 1 μJ and 50 Ω, respectively. To receive echo signals, the Panametrics-NDT 5900PR was set with a bandpass filter from 10 to 20 MHz and a gain of 40 dB, which were applied before analog signals were digitized via a GaGe EON CompuScope CS122G1 Digitizer (Dynamic Signals, LLC, Lockport, IL, USA) with a 1-GS/s sampling rate.

Insertion loss (IL) was measured by immersing the SL-ERUS phased-array transducer catheter in a deionized water tank, exciting each element in the array with a 5-Vpp, 30-cycle sinusoidal tone-burst signal generated by a Tektronix AFG 3252 Dual Channel Arbitrary/Function Generator (Tektronix, Inc., Beaverton, OR, USA) at the array center frequency, and receiving the reflected echo from a polished quartz reflector placed at the elevation natural focal distance. Measured echo signals were divided by the input signal and the resulting quotients were expressed in decibels. Afterward, these results were corrected for loss due to attenuation in water ($\alpha = 2.0 \times 10^{-4}$ dB/mm $\cdot$ MHz^2) and reflection from the quartz target (1.9 dB) [13], [20].

C. Combined Electrical and Acoustical Crosstalk

Combined electrical and acoustical crosstalk measurements were performed by immersing the SL-ERUS phased-array transducer catheter in a deionized water tank with no polished quartz reflector. A Tektronix AFG 3252 Dual Channel Arbitrary/Function Generator was used to excite one element in the array with a 5-Vpp, 5-cycle sinusoidal tone-burst signal within a frequency range from 2 to 30 MHz in steps of 2 MHz. The applied signal was measured with a LeCroy LC534 1-GHz Oscilloscope (LeCroy Corporation, Chestnut Ridge, NY, USA) and served as a reference to the measured signals from four adjacent elements. These measurements were executed on element 18 with respective adjacent elements 17, 16, 15, and 14, as well as on element 37 with respective adjacent elements 36, 35, 34, and 33. Afterward, the crosstalk for the first adjacent elements, the second adjacent elements, the third adjacent elements, and the fourth adjacent elements was averaged and plotted as relative amplitudes.

D. Single-Element Azimuthal Directivity Response

The one-way azimuthal directivity response was measured by exciting a representative array element with a 50-Vpp, 5-cycle sinusoidal tone-burst signal generated by a Tektronix AFG 3252 Dual Channel Arbitrary/Function Generator connected to an Amplifier Research 50W1000B solid-state power amplifier (Amplifier Research, Inc., Souderton, PA, USA). A needle hydrophone HGL-0085 (Onda Corporation, Sunnyvale, CA, USA), placed at the natural elevation focus and connected to a LeCroy WaveRunner 104MXi 1-GHz Oscilloscope, was used to acquire the amplitude of the time-domain response at discrete angular positions. The effective element width was estimated by matching a theoretical directivity curve to the measured values [13], [21].

V. Array Transducer Imaging

The ultimate performance indicators of the SL-ERUS phased-array transducer catheter were determined by its imaging capability of three different kinds of targets using a Verasonics Vantage 128 System.

Imaging was performed acquiring 128 ray lines in a phased-array configuration, with each ray line constituting a separate beamformed transmit operation with fixed focus, followed by a respective beamformed receive operation with dynamic focusing, yielding 128 transmit and receive angles spaced at $(\pi/2)/128$.

RF data were acquired at a sampling frequency of 62.5 MHz, with the transmit frequency set to 15.625 MHz, and a three half-cycle pulse transmit waveform.

After all of the individual ray lines were acquired, the image data were reconstructed to yield the phased-array images. The system 40-dB time gain compensation was adjusted to optimize the images for display. No apodization was applied to the array transducer aperture in any of the imaging experiments.

The first target, shown in Fig. 9(a), was a custom-made fine-wire phantom composed of three evenly spaced 20-μm-diameter tungsten wires (California Fine Wire Company, Grover Beach, CA, USA) with the purpose of determining the axial and lateral spatial resolutions of the array transducer. The axial separation between wires was around 1.0 mm, and the azimuth separation was around 1.6 mm. The custom-made fine-wire phantom was immersed in a tank with deionized water. At a center frequency of 15 MHz, the sound wavelength in the transmitting medium is 100 μm; therefore, the wires could safely be assumed as three point targets. The transmit focus was set at a depth of 8 mm with a transmit pulse of 40 Vpp. The acquired image was postprocessed with a scaling gain of 15 dB, and minimal thresholding was used in order to highlight the wire targets.

The second target, shown in Fig. 9(b), was a custom-made colorectal tissue-mimicking phantom composed of urethane rubber ($\alpha = 0.5$ dB/cm-MHz, $c = 1450$ m/s) (Supertech, Inc., Elkhart, IN, USA) into which a 700-μm-diameter stainless steel needle was inserted with the purpose of demonstrating the capability of the array transducer to detect solid structures embedded in tissue. The custom-made colorectal tissue-mimicking phantom was immersed in a tank with

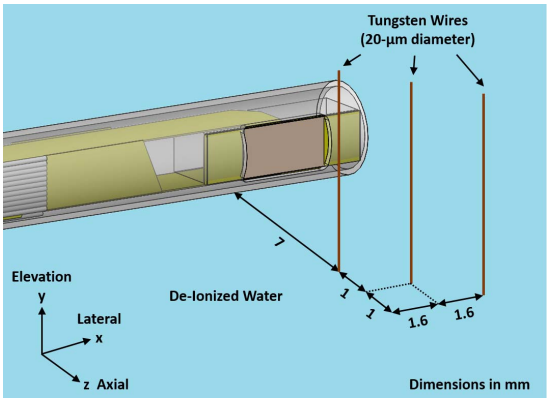

(a)

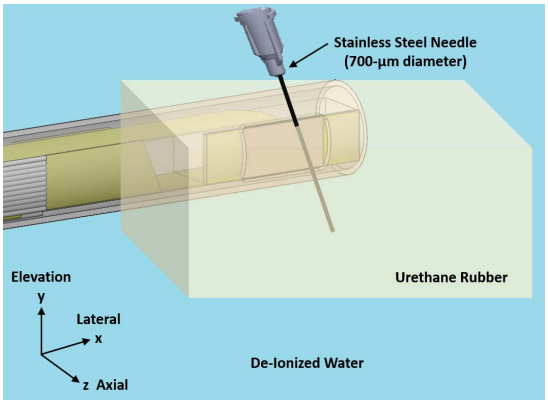

(b)

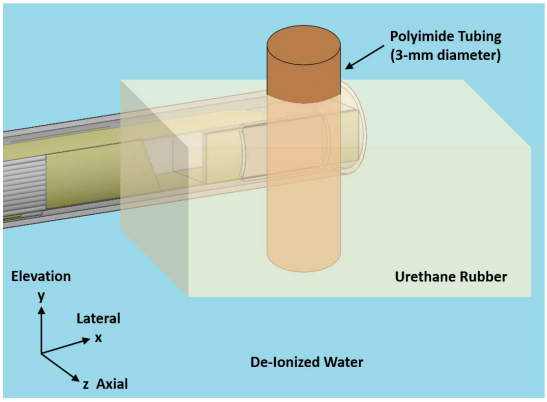

(c)

Fig. 9. Targets for imaging experiments of the SL-ERUS phased-array transducer catheter. (a) Custom-made fine-wire phantom. (b) Custom-made colorectal tissue-mimicking phantom with an inserted 700-μm-diameter stainless steel needle. (c) Custom-made colorectal tissue-mimicking phantom with an inserted piece of 3-mm-diameter polyimide tubing. All targets were immersed in a tank with deionized water during the imaging experiments.

deionized water. The transmit focus was set at a depth of 12 mm with a transmit pulse of 40 Vpp. The acquired images were postprocessed with a scaling gain of 26 dB.

The third and last target, shown in Fig. 9(c), was a custom-made colorectal tissue-mimicking phantom composed of urethane rubber into which a piece of 3-mm-diameter polyimide tubing was inserted with the purpose of demonstrating the capability of the array transducer to detect cysts present in tissue. The custom-made colorectal tissue-mimicking phantom

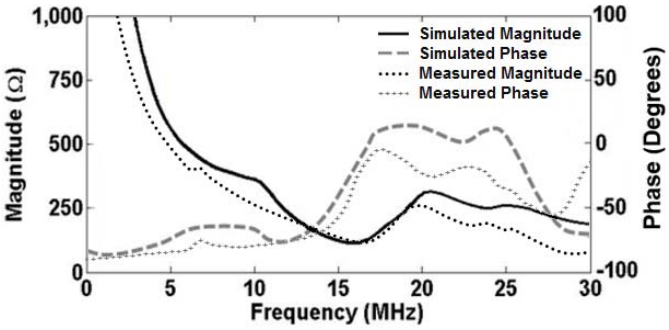

(a)

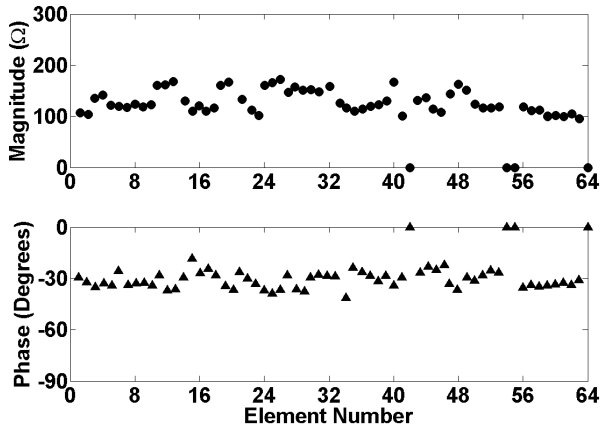

(b)

Fig. 10. (a) Simulated and measured electrical impedance magnitude and phase angle of representative array element 33. (b) Uniformity of electrical impedance magnitude and phase angle of all the phased-array elements.

TABLE IV
COMPARISON OF SIMULATED AND MEASURED ELECTRICAL IMPEDANCE RESULTS

Parameter	PZFlex	Measured
Z @ 15 MHz (Ω)	124.1	129.6 ± 25.3
f_r (MHz)	16.1	16.9 ± 1.5
f_a (MHz)	19.8	20.4 ± 1.8
k_t	0.62	0.60 ± 0.08

was immersed in a tank with deionized water. The transmit focus was set at a depth of 6 mm with a transmit pulse of 40 Vpp. The acquired images were postprocessed with a scaling gain of 22 dB.

VI. Results and Discussion

A. Electrical Impedance

The simulated and measured electrical impedance magnitude and phase angle of a representative array element (element 33) are shown in Fig. 10(a). Element 33 was chosen as representative since its electrical impedance characteristics were closest to the average of all 64 elements.

The simulated and measured results are summarized and compared in Table IV. The measured results showed an electrical impedance magnitude of 129.6 ± 25.3 Ω at 15 MHz.

TABLE V
COMPARISON OF SIMULATED AND MEASURED PULSE-ECHO RESPONSE RESULTS

Parameter	PZFlex	Measured
-6 dB fc (MHz)	14.2 ± 0.7	17.7 ± 1.2
-6 dB BW (%)	54.3 ± 3.1	52.2 ± 9.8
Vpp (mV)	211.3 ± 95.8	200.1 ± 102.7
-6 dB / -20 dB pulse length (ns)	135 / 210	107 / 193
Compensated IL (dB)*	41.7	49.8 ± 3.9

*Simulated value obtained with KLM modeling for a single array element.

The series (f_r) and parallel (f_a) resonant frequencies were 16.9 ± 1.5 MHz and 20.4 ± 1.8 MHz, respectively, yielding an electromechanical coupling coefficient (k_t) of 0.60 ± 0.08 and determined according to the expression [22]

$$k_t = \sqrt{\frac{\pi}{2}\frac{f_r}{f_a}\tan\left[\frac{\pi}{2}\left(\frac{f_a - f_r}{f_a}\right)\right]} \tag{2}$$

The uniformity of the measured values of electrical impedance magnitude and phase angle of all the array elements at 15 MHz is shown in Fig. 10(b). As it can be seen, only four elements presented a short circuit to ground: 42, 54, 55, and 64. The average and standard deviation of the array elements electrical impedance magnitude and phase angle were (129.6 ± 25.3 Ω) and (−33.2° ± 6.1°), respectively.

B. Pulse-Echo Response and Insertion Loss

The simulated and measured pulse-echo responses of a representative array element (element 37) are shown in Fig. 11(a) and (b), respectively. Element 37 was chosen as representative since its pulse-echo response characteristics were closest to the average of all 64 elements.

The simulated and measured results are summarized and compared in Table V. The measured results showed an effective −6-dB center frequency (−6-dB fc) of 17.7 ± 1.2 MHz, a −6-dB fractional BW (−6-dB BW) of 52.2% ± 9.8%, a peak-to-peak sensitivity (Vpp) of 200.1 ± 102.7 mV, and a compensated IL of 49.8 ± 3.9 dB.

The increase in center frequency resulted from slightly overlapping the 2–2 composite by hand, which consequently resulted in shorter −6-dB/−20-dB PLs. The slight decrease in sensitivity resulted mainly from the array elements not having their entire bottom surface perfectly connected to their respective electrodes on the flexible circuit, as it was the case of the FEA simulation model. In reality, the resulting Epo-Tek 301 epoxy thin bonding layer was not perfectly uniform after the clamping process. This can be verified by closely examining the cross-sectional image of the array acoustic stack shown in Fig. 6(b) and by observing the peak-to-peak sensitivity uniformity shown in Fig. 11(c), which clearly indicates how the second half of the array (elements 33 to 64) was better connected to the flexible printed circuit by showing higher peak-to-peak sensitivities than the first 32 elements.

The measured compensated IL was higher than that reported for other linear phased arrays with similar construction; however, the element footprint and, consequently, the dimensions

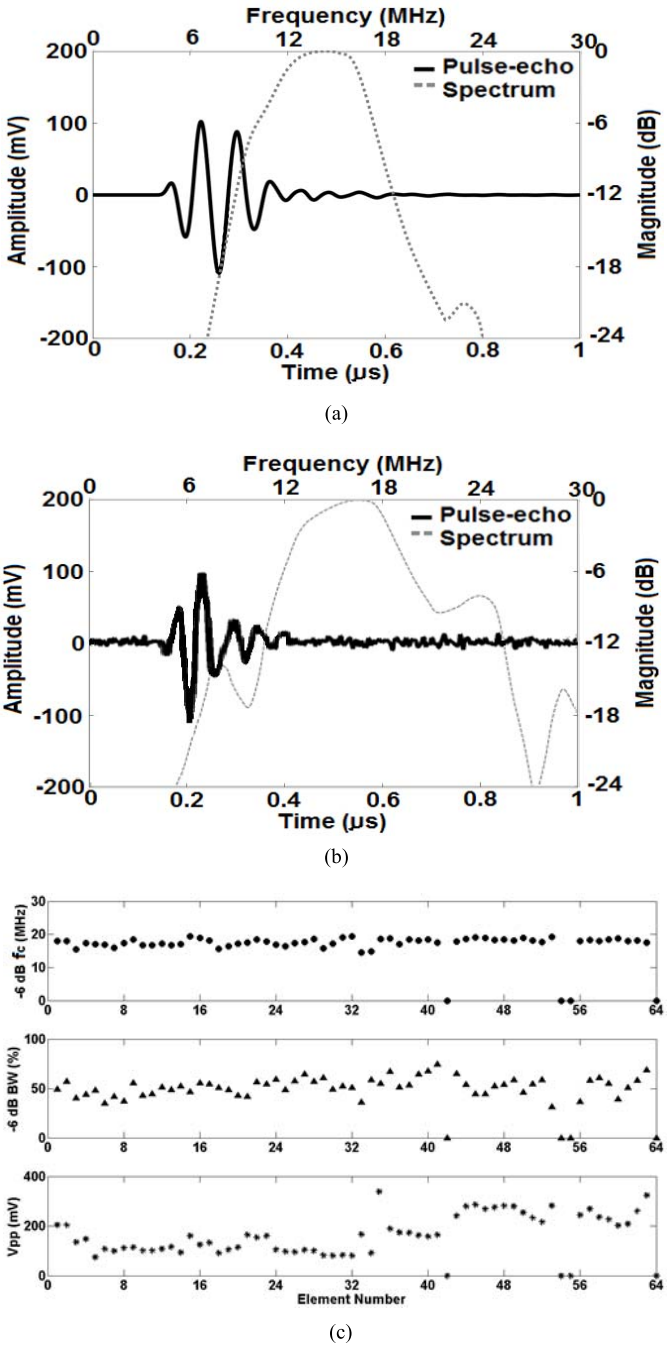

Fig. 11. (a) Simulated and (b) measured pulse-echo responses of representative array element 37. (c) Uniformity of −6-dB center frequency, −6-dB fractional BW, and peak-to-peak sensitivity of all the phased-array elements.

of the signal electrodes on the flexible printed circuit in this array were at least two times smaller, making it more difficult to ensure a perfect connection between the bottom surface of the array elements and their respective flexible circuit signal electrodes. For example, the SL phased-array transducer developed by Stephens *et al.* [23] featured 64 elements within an aperture of 2.6 mm × 6.4 mm, at a pitch of 100 μm, and a center frequency of 7.25 MHz; whereas the SL phased-array transducer being presented includes the same number of elements within an aperture of 1.8 mm × 3.2 mm, at a pitch of only 50 μm, and a center frequency of 17.7 MHz.

In addition, the 64 individual 48-AWG microcoaxial cables used in the array under discussion were not shielded as a bundle, making them more susceptible to external noise and interference considering that the outer conductor thickness of each microcoaxial cable is 17 μm and the skin depth of copper at 15 MHz is approximately 16.8 μm. For a good shielding effect, the thickness of the outer conductor should be at least five times greater than the skin depth [24]. A solution could be to assemble all 64 microcoaxial cables together with 50-μm binder tape, shield them with 46-AWG braiding, and wrap them with 50-μm fluoropolymer tape [23]. This additional shielding would prevent electromagnetic wave radiation through the outer conductor of each microcoaxial cable; therefore, decreasing IL and improving sensitivity by preserving the signal integrity of the received echo.

To obtain an acceptable SNR in tissue, future versions of the catheter could include impedance transformers or active preamplifiers on each channel, which are commonly used to boost the signal above the noise floor of the system for small elements with high impedance [25]. The uniformity of the measured values of −6-dB center frequency, −6-dB fractional BW, and peak-to-peak sensitivity of all the array elements is shown in Fig. 11(c).

C. Combined Electrical and Acoustical Crosstalk

The simulated and measured crosstalk values are shown in Fig. 12(a) and (b), respectively. As it can be seen, the measured values of crosstalk were found to be comparable to the simulation results. Maximum measured crosstalk values at the array center frequency were −30.5 dB for the first adjacent element, −32.8 dB for the second adjacent element, −34.4 dB for the third adjacent element, and −40.1 dB for the fourth adjacent element; which denote satisfactory but not ideal element-to-element isolation in accordance to the suggested maximum crosstalk design guideline of < -35 dB for phased arrays with a linear configuration [11], [26].

The relatively high crosstalk values for the first and second adjacent elements could be attributed to two main factors: 1) acoustical cross-coupling between consecutive elements in the 2–2 array composite due to the narrow, 13-μm-wide, epoxy-filled kerfs and 2) electrical cross-coupling between consecutive signal electrodes on the flexible printed circuit having a pitch of only 50 μm.

D. Single-Element Azimuthal Directivity Response

The simulated and measured one-way azimuthal directivity responses of representative array element 37 are shown in Fig. 12(c). The measured −6-dB directivity was approximately ±22°. Since the isolation between consecutive elements was not ideal, the effective element width (44 μm) was 19% larger than the actual element width of 37 μm. A similar result was reported by Ritter *et al.* [27] of an effective element width 16% larger than the actual element width for a 30-MHz linear array with maximum crosstalk < -30-dB and −6-dB directivity of ±20°. Similarly, Chiu *et al.* [28] reported a −6-dB directivity of approximately ±20° for a 20-MHz phased array with maximum crosstalk < -28 dB.

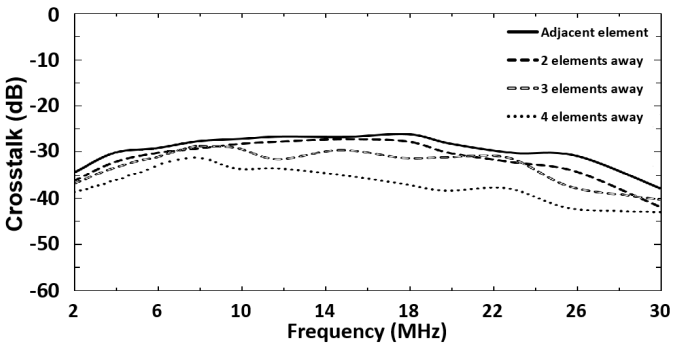

(a)

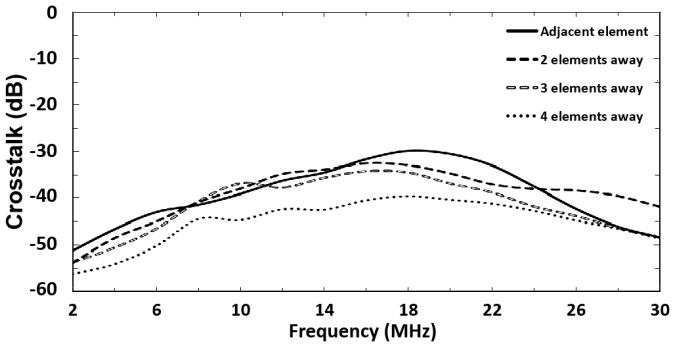

(b)

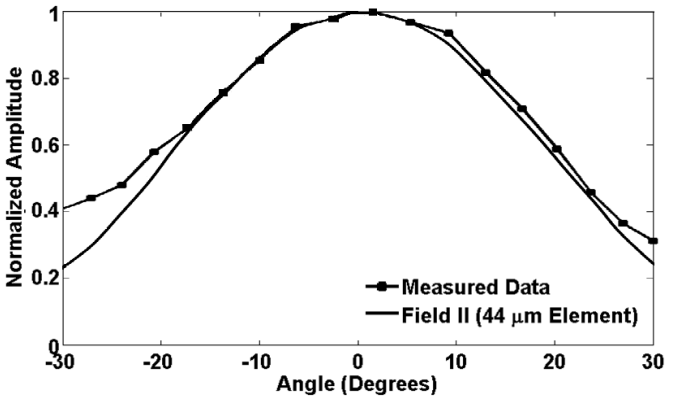

(c)

Fig. 12. (a) Simulated and (b) measured crosstalk values for four nearest neighboring elements in the array. (c) Simulated and measured one-way azimuthal directivity responses of representative array element 37.

E. Array Transducer Imaging

The acquired image of the custom-made fine-wire phantom is shown in Fig. 13(a). As it can be seen, the three wires were clearly visible with reasonable image quality, especially the middle one located at the elevation natural focal distance. Faint artifacts were observed mostly to the left and right sides of the three wires due to the presence of sidelobes in the ultrasound beam. Implementing apodization could have reduced the amplitude of such sidelobes; however, this would have increased the main lobe width, consequently degrading spatial resolutions [29].

Faint artifacts were also observed on the front of the wires mainly due to thickness irregularities of the matching layers, as well as slight wire reverberation and misalignment with

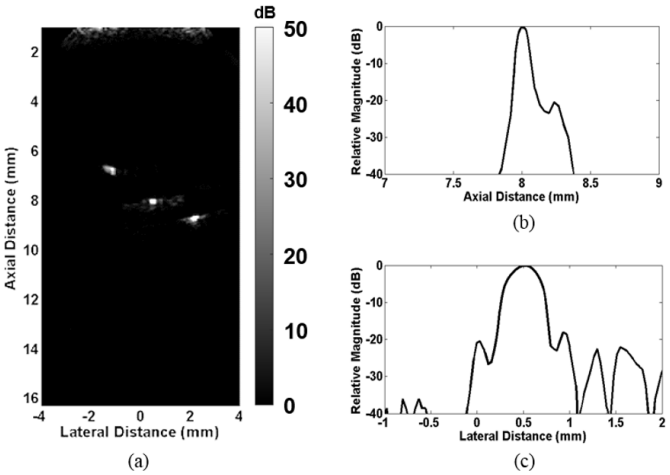

Fig. 13. Imaging of custom-made fine-wire phantom. (a) Acquired image with a dynamic range of 48 dB. (b) Plot of the axial line spread function for the middle wire. (c) Plot of the lateral line spread function for the middle wire.

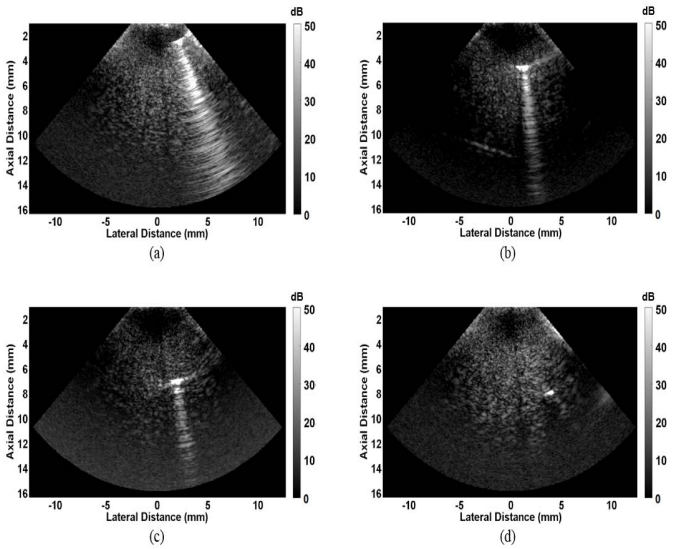

Fig. 14. Imaging of custom-made colorectal tissue-mimicking phantom with an inserted stainless steel needle. Images have a dynamic range of 48 dB. (a) Needle inserted at a depth of 3 mm and oblique across the array transducer azimuth aperture. (b) Needle inserted at a depth of 5 mm and oblique across the array transducer azimuth aperture. (c) Needle inserted at a depth of 8 mm and oblique across the array transducer azimuth aperture. (d) Needle inserted at a depth of 8 mm and parallel across the array transducer elevation aperture.

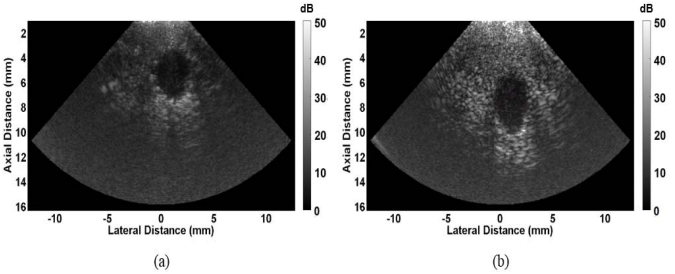

Fig. 15. Imaging of custom-made colorectal tissue-mimicking phantom with an inserted piece of polyimide tubing. Images have a dynamic range of 48 dB. (a) Piece of polyimide tubing inserted at a depth of 5 mm and parallel across the array transducer elevation aperture. (b) Piece of polyimide tubing inserted at a depth of 8 mm and parallel across the array transducer elevation aperture.

respect to the array transducer elevation aperture. The plots of the axial and lateral line spread functions for the middle wire are shown in Fig. 13(b) and (c), respectively.

The measured full-width half-maximum (FWHM) spatial resolutions were approximately 90 and 420 μm in the axial and lateral directions, respectively. These measurements correlated well with the theoretical axial (80.25 μm) and lateral (450 μm) spatial resolutions, predicted by the well-known equations $R_A = \text{PL}/2$ and $R_L = F\# \times \lambda$ [30], where R_A and R_L are the axial and lateral spatial resolutions, respectively; PL is the -6-dB spatial pulse length of the received echo from the previous pulse-echo response measurements (measured -6-dB time PL of 0.107 μs corresponds to a -6-dB spatial PL of 160.5 μm), $F\#$ is the F-number of the array transducer aperture defined as the ratio of focal distance to aperture dimension [26], and λ is the sound wavelength in the transmitting medium.

The acquired images of the custom-made colorectal tissue-mimicking phantom with an inserted 700-μm-diameter stainless steel needle are shown in Fig. 14. Fig. 14(a) shows the needle inserted at a depth of approximately 3 mm and oblique across the array transducer azimuth aperture. Fig. 14(b) shows the needle inserted at a depth of approximately 5 mm and oblique across the array transducer azimuth aperture. Fig. 14(c) shows the needle inserted at a depth of approximately 8 mm and oblique across the array transducer azimuth aperture. Fig. 14(d) shows the needle inserted at a depth of approximately 8 mm and parallel across the array transducer elevation aperture.

The acquired images of the custom-made colorectal tissue-mimicking phantom with an inserted piece of 3-mm-diameter polyimide tubing are shown in Fig. 15. Fig. 15(a) shows the cyst resulting from inserting the piece of polyimide tubing at a depth of approximately 5 mm and parallel across the array transducer elevation aperture. Similarly, Fig. 15(b) shows the cyst resulting from inserting the piece of polyimide tubing at a depth of approximately 8 mm and parallel across the array transducer elevation aperture.

VII. Conclusion

This paper described the design, fabrication, and testing of a miniaturized 15-MHz SL phased-array transducer. The 64-element phased-array transducer was fit inside of a 1.5-m-long 10F catheter having an external diameter of 3.3 mm. The device construction enables its potential integration into a novel robotic surgical instrument that combines endomicroscopy and ERUS.

Standard characterization testing confirmed that the array provides adequate peak-to-peak sensitivity ($\geq$100 mV) and spatial resolution (90 μm axially/420 μm laterally). The relatively high crosstalk (≤ -30 dB) may be reduced in the future with the addition of particles or LP to the kerf filling epoxy to increase attenuation between consecutive elements in

the 2–2 composite. Similarly, IL and SNR can be improved by providing the cable assembly with additional shielding and by including impedance transformers or active preamplifiers on each channel, respectively.

Finally, acquired images of custom-made colorectal tissue-mimicking phantoms confirmed that the array provides adequate penetration depth ($\geq$8.1 mm) and demonstrated its capability to detect solid structures and cysts present in the tissue; therefore, confirming its potential suitability to provide intraoperative image guidance and tissue characterization during TEM procedures.

ACKNOWLEDGMENT

The authors would like to thank R. Roth from Hitachi Cable America, Dr. J. Tian from CTS Corporation, and Dr. R. Chen from the Resource Center for Medical Ultrasonic Transducer Technology, University of Southern California (USC), Los Angeles, CA, USA, for their technical suggestions on microcoaxial cabling, PMN-30% PT composites, and array transducer characterization testing, respectively. They also would like to thank the editors and reviewers for their helpful suggestions.

REFERENCES

[1] A. Cuschieri, "Technology for minimal access surgery," *BMJ*, vol. 319, no. 7220, p. 1304, Nov. 1999.

[2] V. Ignatov *et al.*, "Diagnostic modalities in colorectal cancer–endoscopy, Ct and pet scanning, magnetic resonance imaging (MRI), endoluminal ultrasound and intraoperative ultrasound," in *Colorectal Cancer-Surgery, Diagnostics and Treatment*. Rijeka, Croatia: InTech, Mar. 2014, pp. 29–51.

[3] R. J. Dickinson and R. I. Kitney, "Miniature ultrasonic probe construction for minimal access surgery," *Phys. Med. Biol.*, vol. 49, no. 16, p. 3527, Aug. 2004.

[4] T. Cummins, P. Eliahoo, and K. K. Shung, "High-frequency ultrasound array designed for ultrasound-guided breast biopsy," *IEEE Trans. Ultrason., Ferroelectr., Freq. Control*, vol. 63, no. 6, pp. 817–827, Jun. 2016.

[5] Y. Yang *et al.*, "Integrated optical coherence tomography, ultrasound and photoacoustic imaging for ovarian tissue characterization," *Biomed. Opt. Express*, vol. 2, no. 9, pp. 2551–2561, 2011.

[6] K. Masamune and J. Hong, "Advanced imaging and robotics technologies for medical applications," *Int. J. Optomechatronics*, vol. 5, no. 4, pp. 299–321, Dec. 2011.

[7] G. Dwyer, P. Giataganas, P. Pratt, M. Hughes, and G.-Z. Yang, "A miniaturised robotic probe for real-time intraoperative fusion of ultrasound and endomicroscopy," in *Proc. IEEE ICRA*, Seattle, WA, USA, May 2015, pp. 1196–1201.

[8] B. R. Edelman and M. R. Weiser, "Endorectal ultrasound: Its role in the diagnosis and treatment of rectal cancer," *Clin. Colon Rectal Surg.*, vol. 21, no. 3, pp. 167–177, Aug. 2008.

[9] S. J. Choi, H.-S. Kim, S.-J. Ahn, Y. M. Jeong, and H.-Y. Choi, "Evaluation of the growth pattern of carcinoma of colon and rectum by MDCT," *Acta Radiol.*, vol. 54, no. 5, pp. 487–492, Jun. 2013.

[10] Y. Chen *et al.*, "High frequency PMN-PT single crystal focusing transducer fabricated by a mechanical dimpling technique," *Ultrasonics*, vol. 53, no. 2, pp. 345–349, Feb. 2013.

[11] R. E. McKeighen, "Design guidelines for medical ultrasonic arrays," *Proc. SPIE*, vol. 3341, pp. 2–19, May 1998.

[12] D. M. Pozar, "Transmission line theory," in *Microwaye Engenering*, 4th ed. Hoboken, NJ, USA: Wiley, 2012, pp. 48–94.

[13] J. M. Cannata, J. A. Williams, Q. Zhou, T. A. Ritter, and K. K. Shung, "Development of a 35-MHz piezo-composite ultrasound array for medical imaging," *IEEE Trans. Ultrason., Ferroelectr., Freq. Control*, vol. 53, no. 1, pp. 224–236, Jan. 2006.

[14] C. S. Desilets, J. D. Fraser, and G. S. Kino, "The design of efficient broad-band piezoelectric transducers," *IEEE Trans. Sonics Ultrason.*, vol. 25, no. 3, pp. 115–125, May 1978.

[15] D. M. Pozar, "Microwave network analysis," in *Microwave Engineering*, 4th ed. Hoboken, NJ, USA: Wiley, 2012, pp. 165–227.

[16] R. Chen *et al.*, "PMN-PT single-crystal high-frequency kerfless phased array," *IEEE Trans. Ultrason., Ferroelectr., Freq. Control*, vol. 61, no. 6, pp. 1033–1041, Jun. 2014.

[17] J. A. Jensen, "FIELD: A program for simulating ultrasound systems," in *Proc. IEEE 10th Nordic-Baltic Conf. Biomed. Imag.*, vol. 4, Mar. 1996, pp. 351–353.

[18] H. P. Savakus, K. A. Klicker, and R. E. Newnham, "PZT-epoxy piezoelectric transducers: A simplified fabrication procedure," *Mater. Res. Bull.*, vol. 16, no. 6, pp. 677–680, Jun. 1981.

[19] H. Wolf, H. Gieser, and L. Maurer, "Transmission lines on flexible substrates with minimized dispersion and losses," in *Proc. Eur. Microw. Conf.*, Nuremberg, Germany, Oct. 2013, pp. 448–451.

[20] G. R. Lockwood, D. H. Turnbull, and F. S. Foster, "Fabrication of high frequency spherically shaped ceramic transducers," *IEEE Trans. Ultrason., Ferroelectr., Freq. Control*, vol. 41, no. 2, pp. 231–235, Mar. 1994.

[21] J. M. Cannata, J. A. Williams, and K. K. Shung, "A kerfless 30 MHz linear ultrasonic array," in *Proc. IEEE Ultrason. Symp.*, Rotterdam, The Netherlands, Sep. 2005, pp. 109–112.

[22] R. Krimholtz, D. A. Leedom, and G. L. Matthaei, "New equivalent circuits for elementary piezoelectric transducers," *Electron. Lett.*, vol. 6, no. 13, pp. 398–399, Jun. 1970.

[23] D. N. Stephens *et al.*, "Donnell, and D. J. Sahn, "The acoustic lens design and *in vivo* use of a multifunctional catheter combining intracardiac ultrasound imaging and electrophysiology sensing," *IEEE Trans. Ultrason., Ferroelectr., Freq. Control*, vol. 55, no. 3, pp. 602–618, Mar. 2008.

[24] J. Lienig and H. Bruemmer, "Electromagnetic compatibility (EMC)," in *Fundamentals of Electronic Systems Design*, 1st ed. Cham, Switzerland: Springer, 2017, pp. 147–191.

[25] R. L. Goldberg, C. D. Emery, and S. W. Smith, "Hybrid multi/single layer array transducers for increased signal-to-noise ratio," *IEEE Trans. Ultrason., Ferroelectr., Freq. Control*, vol. 44, no. 2, pp. 315–325, Mar. 1997.

[26] K. K. Shung and M. Zippuro, "Ultrasonic transducers and arrays," *IEEE Eng. Med. Biol. Mag.*, vol. 15, no. 6, pp. 20–30, Nov./Dec. 1996.

[27] T. A. Ritter, T. R. Shrout, R. Tutwiler, and K. K. Shung, "A 30-MHz piezo-composite ultrasound array for medical imaging applications," *IEEE Trans. Ultrason., Ferroelectr., Freq. Control*, vol. 49, no. 2, pp. 217–230, Feb. 2002.

[28] C. T. Chiu, B. J. Kang, P. Eliahoo, T. Abraham, and K. K. Shung, "Fabrication and characterization of a 20-MHz microlinear phased-array transducer for intervention guidance," *IEEE Trans. Ultrason., Ferroelectr., Freq. Control*, vol. 64, no. 8, pp. 1261–1268, Aug. 2017.

[29] C. H. Frazier and W. D. O'Brien, "Synthetic aperture techniques with a virtual source element," *IEEE Trans. Ultrason., Ferroelectr., Freq. Control*, vol. 45, no. 1, pp. 196–207, Jan. 1998.

[30] F. S. Foster *et al.*, "A new ultrasound instrument for *in vivo* microimaging of mice," *Ultrasound Med. Biol.*, vol. 28, no. 9, pp. 1165–1172, Sep. 2002.

Nestor E. Cabrera-Munoz (S'12–M'18) received the B.S. degree in mechanical-electrical engineering from the Monterrey Institute of Technology, ITESM Campus Monterrey, Mexico, in 2005, and the M.S. degree in biomedical engineering, the Graduate Certificate degree in technology commercialization, and the Ph.D. degree in biomedical engineering from the University of Southern California, Los Angeles, CA, USA, in 2010, 2014, and 2018, respectively, under the supervision of Dr. K. Kirk Shung.

He has professional R&D and project management experience in the areas of heating, ventilation, and air conditioning (HVAC), automotive engineering, and medical devices. His current research interests include the design, modeling, fabrication, and testing of high-frequency ultrasonic transducers and arrays for medical and nondestructive testing applications.

Dr. Cabrera-Munoz is a member of ASME.

Payam Eliahoo is currently pursuing the Ph.D. degree in biomedical engineering with the University of Southern California, Los Angeles, CA, USA.

He is a member of the Ultrasound Transducer Resource Center, Los Angeles, CA, USA. His current research interests include high-frequency ultrasound imaging array electronics development.

Robert Wodnicki (M'09) received the B.Eng. and M.Eng. degrees in electrical engineering from McGill University, Montreal, QC, Canada, in 1992 and 1996, respectively.

From 1995 to 2014, he was an Electrical Engineer with GE Global Research, Niskayuna, NY, USA. He is currently a Graduate Student with the Biomedical Engineering Department, Viterbi Engineering School, University of Southern California, Los Angeles, CA, USA. His research has centered on the implementation of mixed-signal ASIC designs for sensor interface, including the design of ASICs for miniaturization of ultrasound electronics.

Hayong Jung received the B.S. and M.S. degrees in electrical engineering from Kwangwoon University, Seoul, South Korea, in 2007 and 2009, respectively, and the M.S. degree in electrical engineering from the University of Southern California (USC), Los Angeles, CA, USA, in 2013, where he is currently pursuing the Ph.D. degree with the Department of Biomedical Engineering.

He is conducting his research in the National Institutes of Health Ultrasonic Transducer Resource Center (UTRC) on the design of high-frequency ultrasound imaging systems and applications under the direction of Dr. K. Kirk Shung.

Chi Tat Chiu received the bachelor's degree in medical engineering and the master's degree in electrical and electronic engineering from The University of Hong Kong, Hong Kong, in 2008 and 2011, respectively, and the Ph.D. degree in biomedical engineering from the University of Southern California, Los Angeles, CA, USA, in 2016, under the supervision of Prof. K. K. Shung.

He is currently an Ultrasound Probes Scientist with the Department of Imaging and Bioelectronics, GE Global Research, Niskayuna, NY, USA. His current research interests include the development of high-frequency ultrasonic transducer arrays, and back-end signal processing, including beamforming and flow imaging.

Jay A. Williams is a retired engineer who previously worked for the NIH Resource on Medical Ultrasonic Transducer Technology for 14 years. In 2002, he joined the Resource Center, University of Southern California, Los Angeles, CA, USA, where he was the Webmaster and he was involved in process development, some transducer/product design, fixture design, and the fabrication of: 128 element 30-MHz composite 30-μm pitch phased arrays, 256 element 30-MHz composite 50-μm pitch linear arrays, 64 element 35-MHz composite 50-μm pitch linear arrays, 8 element 40–50-MHz copolymer annular arrays, very lightweight (<0.3 g 40–60 MHz, <0.2 g 80–100 MHz) high frame rate b-scan transducers, 100–150-MHz sputtered ZnO transducers, 10-MHz composite HIFU transducers for catheter use, and 64 element 8-MHz composite 100-μm pitch phased arrays for catheter use. In 1990, he began working in ultrasound at Blatek, Inc., State College, PA, USA, serving 8½ years in engineering then 2½ years in management, including 5 years as IS/IT Manager – Net. Admin., and 2 years as Quality System Manager in charge of establishing their first ISO 9001 and FDA CGMP (21CFR820) compliant quality system. He was in the ultrasound field for 25 years. He holds patent no. 7 695 784 covering postpositioning for interdigital bonded composites, USC file 3829. He was involved in industry for 25 years in a variety of technical fields such as mass spectrometry, microwave telecommunication, liquid chromatography, digital electronics, ultrasound, and information technology.

Hyung Ham Kim (M'10) received the B.S. degree in electrical engineering from the Korea Advanced Institute of Science and Technology, Daejeon, South Korea, in 1993, the M.S. degree in electrical engineering from Seoul National University, Seoul, South Korea, in 1995, and the M.S. and Ph.D. degrees in biomedical engineering from the University of Southern California at Los Angeles, Los Angeles, CA, USA, in 2006 and 2010, respectively.

He was a Research Assistant Professor with the Department of Biomedical Engineering, University of Southern California and the Manager of the NIH Resource Center for Medical Ultrasonic Transducer Technology, University of Southern California, Los Angeles. In 2014, he joined Analogic Inc., Peabody, MA, USA. He was the Manager and Principal Engineer in the Probe Department, Medison Co., Ltd., Seoul, South Korea, from 1994 to 2004, where he was involved in research and development projects of medical ultrasound array transducers. In 2016, he was the Director of Business Development with Analogic, where he led the research solutions business. He is currently an Associate Professor with the Department of Creative IT Engineering, Pohang University of Science and Technology (POSTECH), Pohang, South Korea. His current research interests include high-frequency array transducers for high-resolution ultrasound imaging, cellular mechanism studies using high-frequency ultrasound, and neuromodulation using focused ultrasound.

Qifa Zhou (F'19) received the Ph.D. degree from the Department of Electronic Materials and Engineering, Xi'an Jiaotong University, Xi'an, China, in 1993.

In 2002, he joined the Department of Physics, Sun Yat-Sen University, Guangzhou, China, the Department of Applied Physics, Hong Kong Polytechnic University, Hong Kong, and the Materials Research Laboratory, Pennsylvania State University, State College, PA, USA. He is currently a Professor of Ophthalmology and Biomedical Engineering, University of Southern California, Los Angeles, CA, USA. His research interests include the development of piezoelectric high-frequency ultrasonic transducers for biomedical ultrasound and photoacoustic imaging, including intravascular imaging, cancer imaging, and ophthalmic imaging, actively exploring ultrasonic mediated therapeutic technology, including trans-sclera drug delivery, as well as ultrasound for retinal and brain stimulation. He has authored or coauthored more than 200 peer-reviewed articles in journals, including *Nature Medicine*, *Nature Communication*, *Advanced Materials*, and IEEE UFFC.

Dr. Zhou is a fellow of the International Society for Optics and Photonics (SPIE) and the American Institute for Medical and Biological Engineering (AIMBE). He is a member of the Technical Program Committee of the IEEE International Ultrasonics Symposium. He is an Associate Editor of the IEEE TRANSACTIONS ON ULTRASONICS, FERROELECTRICS, AND FREQUENCY CONTROL.

Guang-Zhong Yang (S'90–M'91–SM'08–F'11) is the Director and Co-Founder of the Hamlyn Centre for Robotic Surgery, and Chairman of the UK-RAS Network. The mission of the UK-RAS Network is to provide academic leadership in RAS, expand collaboration with industry and integrate and coordinate activities of the EPSRC funded RAS capital facilities, Centres for Doctoral Training (CDTs), and partner universities across the U.K. His main research interests include medical imaging, sensing and robotics.

Dr. Yang is a fellow of the Royal Academy of Engineering, IET, and AIMBE, MICCAI, and CGI. He was a recipient of the Royal Society Research Merit Award and listed in The Times Eureka Top 100 in British Science.

K. Kirk Shung (S'73–M'75–SM'89–F'93–LF'11) received the B.S. degree in electrical engineering (EE) from Cheng Kung University, Tainan, Taiwan, in 1968, and the Ph.D. degree in EE from the University of Washington, Seattle, WA, USA, in 1975.

Since 2002, he has been a Professor of biomedical engineering with USC, where he has been the Director of NIH Resource Center on Medical Ultrasonic Transducer Technology since 1997. In 2013, he joined the Viterbi School of Engineering, USC, as a Dean's Professor of biomedical engineering. He has authored or coauthored more than 500 papers and book chapters. His research interests include ultrasonic transducers, high-frequency ultrasonic imaging, and ultrasound microbeam.

Dr. Shung is a fellow of American Institute of Ultrasound in Medicine. He is a Founding Fellow of American Institute of Medical and Biological Engineering. He was a recipient of the IEEE Engineering in Medicine and Biology Society Early Career Award in 1985 and was the coauthor of a paper that received the Best Paper Award for IEEE TRANSACTIONS ON ULTRASONICS, FERROELECTRICS, AND FREQUENCY CONTROL (UFFC) in 2000. He was elected an outstanding alumnus of Cheng-Kung University in Taiwan in 2001, and received the Holmes Pioneer Award in Basic Science from American Institute of Ultrasound in Medicine in 2010, the Academic Career Achievement Award from the IEEE Engineering in Medicine and Biology Society in 2011, and the IEEE Biomedical Engineering Award in 2016. He is an Associate Editor of the IEEE TRANSACTIONS ON ULTRASONICS, FERROELECTRICS, AND FREQUENCY CONTROL, and the IEEE TRANSACTIONS ON BIOMEDICAL ENGINEERING AND MEDICAL PHYSICS. He was selected as the Distinguished Lecturer for the IEEE UFFC Society for 2002–2003.